18th Australasian Fluid Mechanics Conference
Launceston, Australia
3-7 December 2012

Numerical Analysis of a Non-Profiled Plate for Flapping Wing Turbines

C.O. Usoh, J. Young, J.C.S. Lai and M.A. Ashraf

School of Engineering and Information Technology
The University of New South Wales, Canberra. ACT 2600, Australia

Abstract

A non-profiled (rectangular) plate section was investigated for its effect on the performance of a flapping wing turbine for power generation. The plate was subjected to laminar flow conditions having a steady free stream flow (Reynolds number *Re* 1100); while flapping with prescribed sinusoidal pitching and plunging kinematics. Results of numerical simulation give a power efficiency as high as 34% for a non-profiled plate with a pitching amplitude of 75^0, a plunge amplitude of 1 chord, a phase difference of 90^0 between pitch and plunge, a reduced frequency 0.8, at pivot location 1/3 chord from the leading edge. This performance is 5.35% over that of the profiled counterpart (NACA0012). Results also show that similar to the profiled plate, the plate thickness has an insignificant effect on the turbine performance.

Introduction

Water and wind are major sources of renewable energy which properly harnessed can significantly contribute towards meeting the increasing demand for clean energy. Both sources are currently underutilised; however the growth rate in utilising wind energy is very prominent when compared to other sources [1]. Oscillating plate/wing turbines are quite new compared to their rotary counterpart. However investigations by Shimizu et al. [2] suggest that oscillating plate turbines have a better performance at low tip speed ratios *TSR* when compared to rotary turbines. The foil sections used in investigations of oscillating plate turbines have been profiled (i.e. streamlined, Figure 1a). Also, the best known efficiency η for a single profiled oscillating plate is between 30% and 40% (Figure 2*)* below the Betz's limit of; 59.3% for a single wind turbine [3].

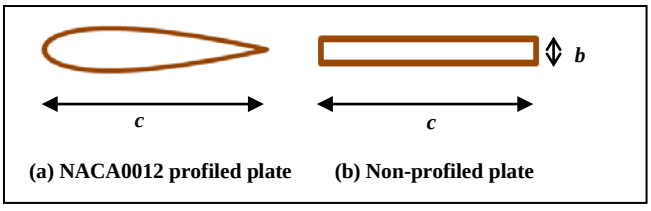

Figure 1. A profiled and non-profiled plate of an oscillating plate turbine

The effects of some kinematic parameters (plunge amplitude h_0, pitch amplitude ϑ_0, phase difference φ, between pitch and plunge, reduced frequency k and pivot location X_p) on the performance of power extraction are summarized in Figure 2. Figure 2 suggests that power extraction in oscillating plate turbines at low *Re* will be at its best for h_0 of 1*c*, φ of 90^0, ϑ_0 of about 70^0, X_p of 1/3*c* or 1/2*c* and k of about 0.9 where c is the chord length. These kinematic conditions promote favourable formation and shedding of the leading edge vortices (LEVs), coupling of the motion of the LEVs and the oscillating plate, energy recovery from the LEVs, in addition to a good synchronisation between the lift force & plunging motion, and the moment force & pitching motion of the plate [4-7].

The design and manufacture of profiled plates are quite complex and costly compared to non-profiled plates. On the other hand, the extent of degradation or improvement on the performance when a non-profiled plate/wing is deployed in an oscillating plate turbine is yet to be ascertained.

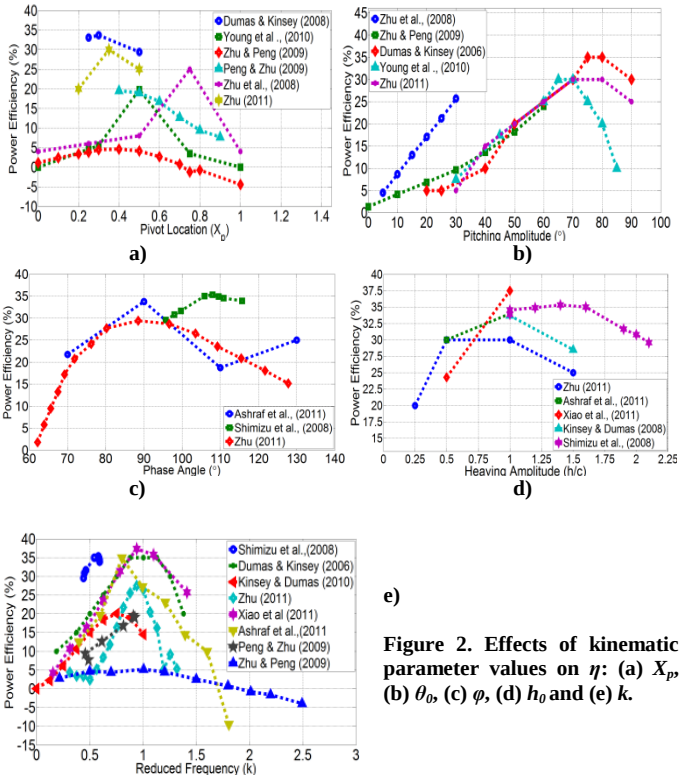

Figure 2. Effects of kinematic parameter values on η: (a) X_p, (b) θ_0, (c) φ, (d) h_0 and (e) k.

The purpose of this study is therefore, to investigate the performance of a non-profiled (rectangular) plate section (Figure 1b) in an oscillating plate turbine. The rectangular plate has the same chord length (c = 1.0m) and cross-sectional area (0.08082m^2) as the profiled plate (Figure 1a). Its relative thickness (b = 0.08082 chord) will be varied to determine its effect on the overall performance. Numerical simulations are conducted using the commercial software package ANSYS 14 FLUENT to solve the unsteady 2D Navier-Stokes equations with prescribed motion kinematics for both pitch and plunge motions, at a low Reynolds number (*Re*) of 1100 for a steady free-stream flow. The *Re* chosen allows comparison with the results in the literature; and for this *Re* the flow can be assumed to be laminar.

Motion Kinematics

The oscillating non-profiled plate is set to undergo a sinusoidal motion in both plunging (*y*-direction) and pitching (about *z*-direction) directions. The plate was pivoted at X_p and restricted to pitch about an angle ϑ_0 while plunging about a defined vertical distance h_0. The phase difference φ of 90^0 was implemented between both motions with the plunge motion $h(t)$ leading the pitch motion $\vartheta(t)$ (equation 1& 2). Figure 3 shows the details of a combined pitch and plunge motion for power extraction over one

periodic cycle when a phase difference φ of 90^0 is implemented between the pitch and plunge.

$$\vartheta(t) = \vartheta_0 \sin(\omega t) \text{ ---- } \Omega(t) = \vartheta_0\, \omega \cos(\omega t) \quad (1)$$

$$h(t) = h_0 \cos(\omega t) \text{ ---- } V_y(t) = -h_0\, \omega \sin(\omega t) \quad (2)$$

where $\Omega(t)$ represents the pitching velocity, $V_y(t)$ the plunging velocity in the y-direction, ω the angular frequency of the oscillation.

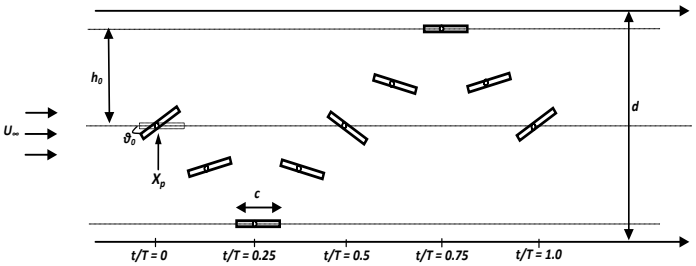

Figure 3. Kinematic motion of a non-profile plate over one cycle

When the non-profiled plate is subjected to pitch and plunge motions defined in equations (1) & (2), the instantaneous effective angle of attack of the plate $\alpha_{eff}(t)$ is given by

$$\alpha_{eff}(t) = \alpha_0 + \vartheta(t) + \tan^{-1}\left(\frac{-V(t)}{U_\infty}\right) \quad (3)$$

where U_∞ is the free stream velocity. The non-dimensional reduced frequency k of the oscillating plate is given by

$$k = \frac{2\pi f c}{U_\infty} = \frac{\omega c}{U_\infty} \quad (4)$$

Energy Extraction and Efficiency

The amount of power p extracted by the oscillating plate turbine is measured by its power coefficient C_p given in terms of equations (5) and (6) respectively. Its efficiency η is defined in equation (7) as the ratio of the extracted power to the available power within the swept area.

$$P(t) = P_h(t) + P_\vartheta(t) = [L.V_y](t) + [M.\Omega](t) \quad (5)$$

$$C_p = \frac{P}{\frac{1}{2}\rho U_\infty^3 sc} = \left[C_{p(\vartheta)} + C_{p(h)}\right](t) =$$

$$\left[C_M.\frac{\Omega.c}{U_\infty} + C_L.\frac{V_y}{U_\infty}\right](t) \quad (6)$$

$$\eta = \frac{P}{\frac{1}{2}\rho U_\infty^3 ds} = C_{p\,(m)}\frac{c}{d} \quad (7)$$

$$d = max\{h_0,\ (h_0 + LE\ \sin\vartheta_0)\ or\ (h_0 - TE\ \sin\vartheta_0)\} \quad (8)$$

Here the span s has a unit value for 2D calculations; ρ, L and M represent density, lift and moment forces respectively; $C_{p(\vartheta)}$ and $C_{p(h)}$ represent the power coefficient for the pitch and plunge motions, while C_M and C_L represent the coefficient of moment and lift respectively. The overall displacement of the plate d is taken as the maximum displacement from either the leading edge LE, trailing edge TE or plunge amplitude h_0 of the oscillating plate over a cycle.

Unsteady Flow Solver

All numerical simulations were undertaken using ANSYS 14 FLUENT CFD commercial software to solve the unsteady incompressible 2D Navier-Stokes equations for laminar free stream flow. The Pressure based solver was selected, adopting the SIMPLE pressure-velocity coupling solution method and Green-Gauss node based gradient. The residual level was set at 10^{-6}; second order scheme was set for pressure while second order upwind scheme set for the momentum to achieve higher-order accuracy.

Two fluid domains centred at the plate's pivot point were modelled to enclose the plate, with a circular domain positioned in-between the square domain (Figure 4). The circular domain bounded by a sliding interface has a radius of 10, while the dimension of each side of the square domain is 70. As employed in [5, 7], a source term method was adopted enabling the use of second order implicit central differencing scheme in time rather than the default first order implicit method deployed in the dynamic mesh strategy whose accuracy is quite limited to fine mesh and very small time-steps. In the source term method adopted, the circular domain containing the plate was made a moving frame thus revolving about the pivot location while the square domain was made a fixed frame. At the inlet boundary, the free stream velocity was applied in the x-direction while the transient plunge velocity was applied in the y-direction. The source term in form of the product of the plunging acceleration and density was added to the Navier-Stokes equation, and applied to both domains in the y-direction using the y-momentum option.

Description of Grid

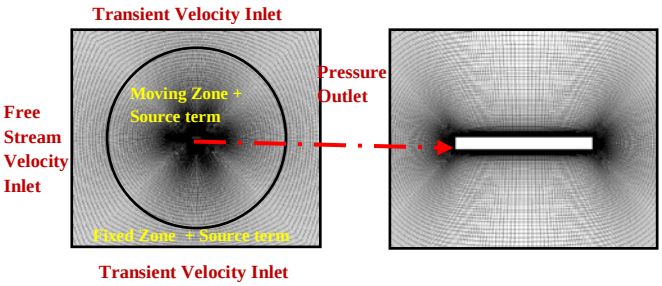

Figure 4. Details of grid, domain zones and boundary conditions

A structured quad-grid (Figure 4) was used to discritize both domains. Three different sets of structured grids were used for grid independence tests: a coarse-grid of 65,000 cells & 450 nodes on the plate, a medium-grid of 121,000 cells & 550 nodes on the plate and a fine-grid of 190,400 cells & 700 nodes on the plate; while time-steps of 500, 2000 and 4000 per cycle were used for the time -step independence study. These tests were conducted for X_p = 0.333c, h_0 = 1.0, ϑ_0 = 76.33^0, k = 0.88 and Re 1100. For each test, at least 12 cycles were calculated until the ratio of $C_{p\ mean}$ for the current cycle to that of the previous cycle is less than 0.14%. Table 1 and Figure 5 show the effect of grid resolution and the number of time-steps on the calculated $C_{p\ mean}$ and η. Based on these results, the medium-grid with 2000 time-steps per cycle were used for simulations here.

Grids	Time step/cycle	1st layer thickness	$C_{p\,mean}$	η (%)
Coarse	2000	5.0e-04	0.8748	34.14
Medium	500	3.2e-04	0.8722	34.04
	2000	3.2e-04	0.8665	33.82
	4000	3.2e-04	0.8664	33.81
Fine	2000	2.3e-04	0.8591	33.53

Table 1. Grid and time-step independence study of the non-profiled plate

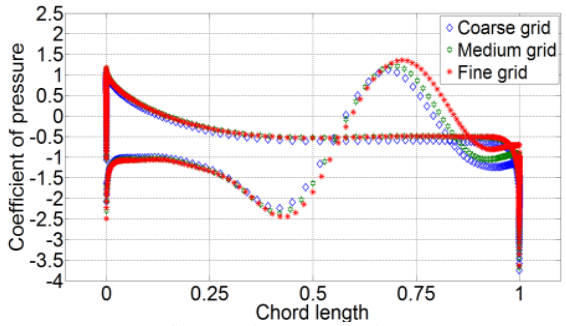

Figure 5. Pressure coefficient of the non-profiled plate section at *t/T* = 0.5 with 2000 time-steps.

Code Validation

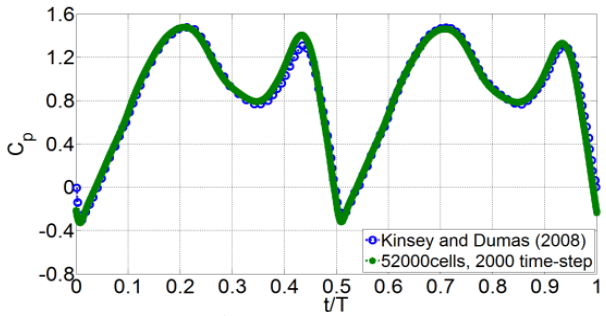

Figure 6. Comparison of C_p with Kinsey and Dumas [5] at X_p = 0.333*c*, h_0 = 1.0*c*, ϑ_0 = 76.33, k = 0.88 & Re = 1100.

The code and methodology adopted here was validated using the numerical results of Kinsey and Dumas [5] for a NACA0015 airfoil at X_p = 0.333*c*, h_0 = 1.0*c*, θ_0 = 76.33, k = 0.88 & Re = 1100. Based on a grid and time-step independence study, a grid of 52,000 cells and 400 nodes around the airfoil was used, with 2000 time-step per cycle. Figure 6 shows that the results obtained ($C_{p\,\text{mean}}$ = 0.8685 & η = 33.89%) agree very well with Kinsey and Dumas [5] ($C_{p\,\text{mean}}$ = 0.860 & η = 33.70%) to within 1%

Results and Discussion

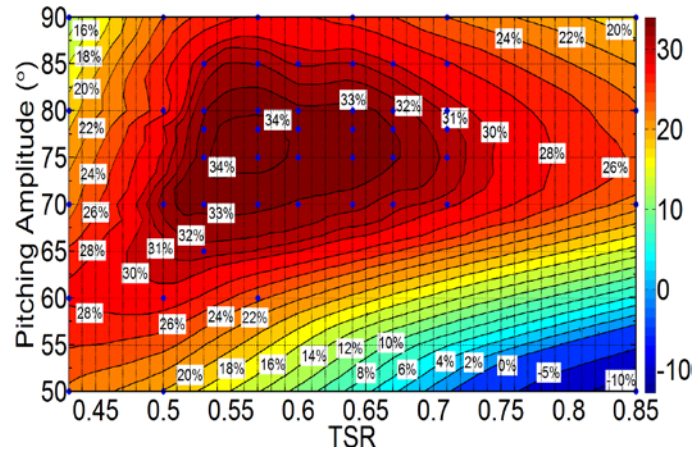

Figure 7. Contour of efficiency η at Re 1100 and X_p 1/3c

Calculations were made for a range of values for ϑ_0 (50^0 to 90^0), k (0.6 to 1.2) with h_0 = 1.0*c*, X_p = 0.333*c* at Re = 1100. The predicted efficiency η contours of the non-profiled plate at different ϑ_0 and *TSR* are given in Figure 7. For the oscillating plate turbine, the *TSR* is related to the instantaneous plunging velocity $V_y(t)$ by

$$TSR = \frac{\omega c}{U_\infty} = \frac{V_{y(rms)}}{U_\infty} \qquad (7)$$

$$V_{y(rms)} = \frac{V_y(t)_{(max)}}{\sqrt{2}} \qquad (8)$$

Efficiencies greater than 33% can be found for *TSR* between 0.53 and 0.66 (i.e. k between 0.75 & 0.93) at ϑ_0 70^0 to 80^0 which is similar to what Kinsey and Dumas [5] reported (k between 0.75 & 1.13 at ϑ_0 70^0 to 80^0) for their NACA0015 analysis.

Re = 1100, X_p = 0.333*c* & ϑ_0 = 75^0	Peak condition k = 0.80, *TSR*= 0.57	
	$C_{p\,mean}$	η %
Non-profiled plate	0.8728	34.23
NACA0012	0.8285	32.49

Table 2. Comparison of $C_{p\,mean}$ and η %of NACA0012 and non-profiled plate at k = 0.80 & θ_0 = 75^0

Calculations were conducted on the observed crests of the performance i.e. *TSR* 0.57 (k = 0.80) at ϑ_0 = 75^0 for the non-profiled plate section and profiled plate (NACA0012) with results (Table 2) showing an improvement in performance as high as 5.35% over the NACA0012 plate. Also a sample of some rotary turbines shows high performance when *TSR* is between 6 & 10; and comparing with Figure 7 where high performance of oscillating turbine is between *TSR* of 0.53 to 0.66, oscillating turbine appears more efficient at low speed flows and low *TSR*. To examine the improvement over the NACA0012 plate, the flow field and pressure coefficient at *t/T* = 0.2, 0.35 and 0.45 were selected for further analysis.

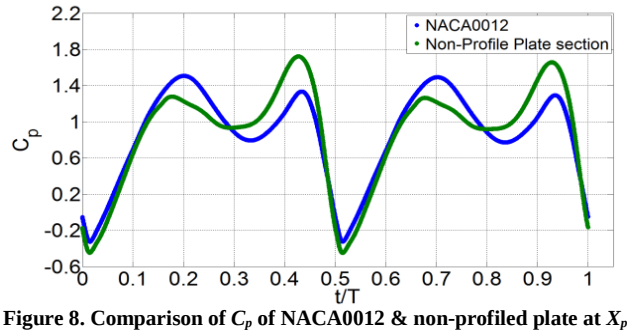

Figure 8. Comparison of C_p of NACA0012 & non-profiled plate at X_p = 0.333*c*, h_0 = 1.0, ϑ_0 = 76.33, k = 0.88 & Re = 1100

The C_p predicted for the non-profiled plate section was lower than that for NACA0012 between *t/T* = 0.15 & 0.30 and 0.65 & 0.80 but higher between *t/T* = 0.30 & 0.45 and 0.80 & 0.95. As shown in Figure 9(a) at *t/T* = 0.20, the plates are pitching in the counter-clockwise direction, the LEV for the non-profiled plate develops earlier than for the NACA0012 plate. This because the sharp edge at the leading edge of the non-profiled plate causes the flow to separate earlier than that in the NACA0012 plate.

Vortex formation in an oscillating plate creates a suction effect due to low pressure on the occurring surface either on the upper or lower surface during the upward/clockwise or downward/counter-clockwise motion of the plate. A well timed LEV is considered to be important for achieving a better synchronisation between the motions and the forces [5, 7, 8]. The pressure coefficient at the leading edge of the NACA0012 plate in Figure 9(c) is lower than the non-profiled plate thus producing a higher adverse pressure gradient in the *y*-direction. The adverse pressure gradient plays a crucial role in determining the direction of the *y*-forces; whether a dynamic stall or lift will be experienced by the body. Thus with the dynamic stall synchronising with the direction of the motions of both plates, there is a reduction in the amount of power required to turn the plate in the counter-clockwise pitching direction in and

in the plunge direction (-*y* direction). Because the pressure gradient is higher at *t/T* = 0.2 & 0.7 for the NACA0012 plate, the power input demanded to move the plate in the pitch and plunge direction is smaller; resulting to a higher power output and efficiency at this point when compared with the non-profiled plate.

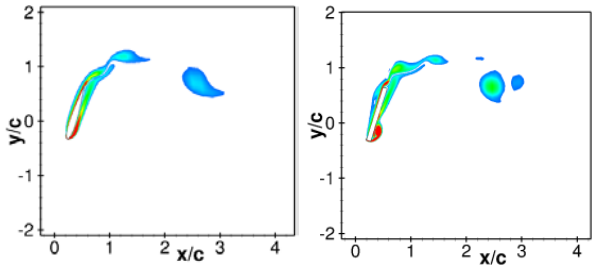

(a) *t/T* = 0.20

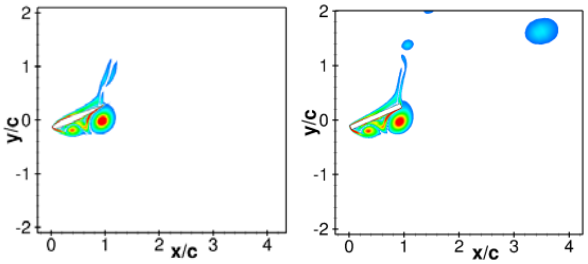

(b) *t/T* = 0.45

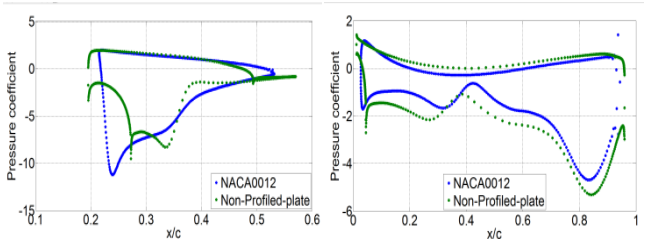

(c) *t/T* = 0.2 **(d) *t/T* = 0.45**

Figure 9. Flow field visualization of vorticity and pressure distribution on the plates at *t/T* = 0.2 & 0.45 for X_p = 0.333*c*, h_0 = 1.0, ϑ_0 = 76.33, *k* = 0.88 & *Re* = 1100.

At *t/T* = 0.35 to 0.45 during the clockwise motion of the plate just before the mid-cycle, when the LEV is fully developed and ready to be shed, the C_p of the non-profiled plate was higher than for the NACA0012 plate. The vortex contours and the pressure coefficient in Figure 9(b) show that the nucleus of the LEV for the non-profiled plate is still closely attached to the lower surface of the plate at *t/T* = 0.45. The straight lower surface (uniform thickness) of the non-profiled plate tends to keep the distance between the boundary layer of the plate and the nucleus of the LEV constant unlike the NACA0012 where the distance increases because of the lower surface curving away from the nucleus of the LEV. This increasing distance between the boundary layer of the plate and the nucleus of the LEV reduces the low pressure on the lower surface of the NACA0012 thus reducing the negative lift force acting on the trailing edge.

These results show that the shape/geometry of the plate affects not only the formation, development and shedding of LEV but also the duration for the attachment and closeness of the nucleus of the LEV to the plate.

Effect of Thickness on Performance

Calculations for the non-profiled plate were made for different thicknesses at $k = 0.90$ & $\theta_0 = 75^0$; 0.5*b* ($C_{p\ mean}$ = 0.8492 & η = 33.30%), *b* ($C_{p\ mean}$ = 0.8621 & η = 33.81%) and 2*b* ($C_{p\ mean}$ = 0.8622 & η = 33.81%). These results show that at $k = 0.90$ & $\theta_0 = 75^0$, the effect of thickness on performance is insignificant, consistent with the study of Kinsey and Dumas [5] for NACA0015 plate. As shown in Figure 9, the instantaneous vortex contours for the 3 non-profiled plates with different thicknesses (2*b*, *b* & 0.5*b*) indicate a close similarity in the formation and shedding of vortices. However, the 2*b* thick plate appears to have slightly larger and fewer numbers of dynamic vortices. Conversely more investigations will be carried out to precisely ascertain this view.

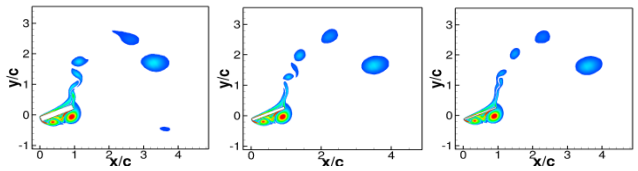

(a) 2*b* **(b) *b*** **(c) 0.5*b***

Figure 9. Instantaneous vortices at *t/T* = 0.45 for thickness (a) 2*b*, (b) *b* & (c) 0.5*b* for *k* = 0.90 and $\theta_0 = 75^0$

Conclusion

A non-profiled plate has been shown by 2D CFD simulations at *Re* = 1100 to be 5.35% better in performance for power extraction than its profiled counterpart with a peak C_p of 0.8729 and η = 34.23% at $k = 0.80$ & $\vartheta_0 = 75^0$. Similar to profiled plates, preliminary results show that thickness has a weak effect on the performance of non-profiled plates. These results demonstrate the potential of employing non-profiled plates for flapping wing turbines because of lower manufacturing costs than profiled plates while enhancing the efficiency and extracted power.

As oscillating plate turbines are more efficient than rotary turbines at low speed flows and small *TSR*, they are viable alternatives for energy extraction under these conditions.

References

[1] The-European-Wind-Energy-Association, "Wind Energy - The Facts", 2009.

[2] Shimizu, E., K.a. Isgoai, and S. Obayashi, "Multiobjective Design Study of a Flapping Wing Power Generator". *Journal of Fluids Engineering*, 2008. **130**.

[3] Betz, A., "Introduction to the Theory of Flow Machines."1966, Oxford: Pergamon Press.

[4] Peng, Z. and Q. Zhu, "Energy harvesting through flow-induced oscillations of a foil". *Physics of Fluids*, 2009. **21**(12): p. 123602-1 to 9.

[5] Kinsey, T. and G. Dumas, "Parametric Study of an Oscillating Airfoil in a Power-Extraction Regime". *AIAA Journal*, 2008. **46**(6): p. 1318-1330.

[6] Zhu, Q., "Optimal frequency for flow energy harvesting of a flapping foil". *Journal of Fluid Mechanics*, 2011. **675**: p. 495-517.

[7] Ashraf, M.A., et al., "Numerical Analysis of an Oscillating-Wing Wind and Hydropower Generator". *AIAA Journal*, 2011. **49**(7): p. 1374-1386.

[8] Xiao, Q., et al., "How motion trajectory affects energy extraction performance of a biomimic energy generator with an oscillating foil?". *Renewable Energy*, 2011. **37**(1): p. 61-75.